# Extended X-ray Absorption Fine-Structure Studies of the Internal Aggregate Structure in Lightly Sulfonated Polystyrene. 2. Effect of Uniaxial Orientation

**B. P. Grady† and S. L. Cooper*,‡**

*Department of Chemical Engineering, University of Wisconsin—Madison, Madison, Wisconsin 53706*

*Received October 5, 1993; Revised Manuscript Received May 6, 1994®*

ABSTRACT: Extended X-ray absorption fine-structure (EXAFS) spectra were measured for three uniaxially extended lightly sulfonated polystyrenes, each containing 6.1 mol % sulfonate groups. The X-rays were linearly polarized, which enabled changes in local structure to be monitored parallel and perpendicular to the stretch direction. For the zinc-neutralized material, the metal–oxygen first-shell distance increased parallel to the stretch direction. Also, the Zn–O first-shell bond vectors were aligned in the stretch direction. A simple theoretical description was developed which allowed quantification of the second moment of the orientation function for these bond vectors. In the nickel-neutralized material, the metal–oxygen first-shell distance did not increase, but Ni–O bond vectors also aligned in the stretch direction. The second coordination shell of sulfur atoms seemed to be unaffected by uniaxial orientation. No changes were found in the local coordination environment of the cadmium-neutralized material after uniaxial extension. The results in this paper are interpreted in light of other orientation studies of ionomers and the structures and composition of the unoriented material.

## Introduction

Orientation of polymers and the response of polymers to an externally applied stress is a significant practical problem since many industrially produced structural components have some residual orientation. Also, some high-performance polymers are commercially important because of properties which are related to orientation; for example, many multiphase polymers are utilized in high-stress applications because of their ability to withstand high elongations without sample failure. This ability is governed by the interaction between the two phases.

Ionomers are polymers with a small mole fraction of ionic groups covalently bonded to the polymer backbone. Energetic incompatibility between the nonpolar organic backbone and the polar ionic groups leads to formation of ionic-rich domains which act as both cross-links and reinforcing filler. A significant difference between ionomers and other multiphase polymers is the strength of the ionic associations; the ionic domains remain intact up to the degradation temperature of the polymer. Also, the ionic domains are small compared to the discrete phase in other multiphase polymers since these domains are only 1–2 nm in diameter.[1]

Different aspects of the microstructural response of ionomers to uniaxial deformation have been studied. These prior measurements were made after the samples were allowed to relax for 30 min, and hence the effect of orientation and relaxation could not be independently studied. SAXS studies of PPO (MW = 1000) soft segment based materials with neutralizing cations $Na^+$, $Sr^{2+}$, $Ca^{2+}$, $Ni^{2+}$, and $Cd^{2+}$ showed cation-dependent behavior.[2] For ionomers neutralized with the first three cations, contour plots of the scattered intensity were ellipsoidal with the meridional peak shifted slightly toward lower $q$ and the equatorial peak shifted slightly toward higher $q$ ($q = 4\pi \sin\theta/\lambda$). Qualitatively, steep increase occurred at low draw ratios (final length/initial length) followed by less severe changes. In fact, the response may reach a maximum near $\lambda = 1.5$–2 and decrease slightly at higher elongations. The patterns corresponding to $Ni^{2+}$ and $Cd^{2+}$ showed no anisotropy at draw ratios from 1 to 3.

Uniaxially deformed, contrast-matched PTMO/TDI materials neutralized with sodium were investigated in SANS experiments.[3] For the PTMO-1000 material, SANS patterns were isotropic until a draw ratio of 1.75, while patterns for the PTMO-2000 material were isotropic until $\lambda = 2$. For the PTMO-1000 material, $R_g$ calculated from the meridional scattering is constant as a function of elongation while $R_g$ calculated from the equatorial scattering is slightly smaller than the isotropic $R_g$. $R_g$ for the PTMO-2000 material did not change outside of experimental error as the draw ratio was increased even though the scattered intensity was clearly anisotropic. These results were similar to the SAXS experiments since the response to uniaxial deformation changed qualitatively between a draw ratio of 1.5–2.

Although sulfonated polystyrene was used in the present study, the response of the internal aggregate order to the applied external stress also changed qualitatively between a draw ratio of 1.5–2. However, the samples in the present study were not allowed to relax after stretching since the samples were quickly quenched to room temperature, which is well below the ionomer's $T_g$. In this study, changes were monitored in the local coordination environment about the cation using the technique of extended X-ray absorption fine-structure (EXAFS) spectroscopy.

## Experimental Section

The 6.1 mol % sodium-neutralized sulfonated polystyrene was supplied by R. D. Lundberg of the Exxon Chemical Co. Details of the conversion from the sodium ionomer to the zinc-, nickel-, or cadmium-neutralized ionomer were given in the first paper of this series.[4] Samples were compression molded in a platen press into 4 cm × 1 cm bars at 220 °C using 90 000 N force. Four different molds were used such that the thickness of the deformed sample would have $\mu t \approx 2$ at 100 eV above the K-edge of the cation. However, for the cadmium samples prohibitively thick samples would have been required. The thickest mold (thickness

* Author to whom correspondence should be addressed.
† Present address: School of Chemical Engineering and Materials Science, University of Oklahoma, Norman, OK 73019.
‡ Present address: College of Engineering, University of Delaware, Newark, DE 19716.
® Abstract published in *Advance ACS Abstracts*, September 15, 1994.

0024-9297/94/2227-6635$04.50/0 

= 4.8 mm) was used for all the cadmium-neutralized samples and hence for the highest elongations, $\mu t \approx 1$. The sample bars were placed in a convection oven, heated to 185 °C, and then stretched in a specially designed apparatus which elongates a sample equally from both ends. This temperature was found to be the lowest temperature (±5 °C) at which the samples would stretch without breaking. Even at this temperature, approximately 60% of the nickel samples failed while about 20% of the zinc and cadmium samples failed. The distance between the grips was 2.7 cm, and the sample was extended at a constant draw rate of 3.67 cm/min. Sample were elongated to the desired draw ratio in a nitrogen atmosphere and then quickly removed from the oven and quenched with liquid nitrogen. The total time between stopping the motor and cooling to room temperature was about 20 s. Unstretched samples were subjected to the same thermal history. No visible discoloration of the samples occurred during heating; however, bubbles formed in some samples to a varying degree. There seemed to be little effect of these bubbles on the EXAFS spectra.

K-edge EXAFS spectra were collected at the Cornell High Energy Synchrotron Source (CHESS). Sagittal focusing was used at the nickel and zinc edges so that the beam width at the sample was only 2–3 mm and the minimum sample width was 5 mm. For the cadmium edge, the beam width was restricted with horizontal slits so that the beam width was still about 3 mm. Samples were aligned carefully to ensure that the sample was in the path of the entire beam. Vertical entrance slits (0.5 mm) were used to obtain high-energy resolution. These slits were centered on the most intense portion of the beam to maximize linear polarization of the X-rays. Measurements done on similar beamlines at CHESS indicate that under these conditions the polarization efficiency is about 95%.[5]

In the preedge region and the EXAFS region, 5 eV steps were used, while 2 eV steps were employed from 20 eV below the edge to 60 eV above the edge. Energy calibrations were performed with the pure metal foils. A 15 cm ionization chamber filled with $N_2$ and a 30 cm ionization chamber filled with Ar, both at 1 atm, were used to monitor the incoming and outgoing intensities of X-rays respectively for the nickel and zinc edges. Because of the higher energy, both ionization chambers were filled with Ar gas for the Cd edge. A total of 12 scans (each lasted ~10 min) were collected, and these scans were added (after $E_0$ determination) before data analysis to improve the signal to noise ratio. Two sets of scans were collected for each sample: one with the draw direction parallel to the electric field vector and one with the two perpendicular.

## EXAFS Theory and Data Analysis

The fundamental equation of EXAFS spectroscopy is

$$\chi(k) = \frac{\mu(E) - \mu_0(E)}{\mu_0(E)} = \sum_j \sum_l 3\cos^2\theta_{lj} \times S_0^2(k)\frac{F_j(k)}{kR_j^2} e^{-2\sigma_j^2 k^2} e^{-2R_j/\lambda_j} \sin[2kR_j + \phi_{ij}(k)] \quad (1)$$

where $\mu(E)$ and $\mu_0(E)$ are the measured and mean absorption coefficients, respectively, at the energy $E$, $\theta_{lj}$ is the angle between the polarization direction of the X-ray electric field and the bond from the central atom to the $l$th atom in the $j$th coordination shell, $S_0^2(k)$ is the amplitude reduction factor which is due to excitations of electrons other than 1s electrons (for a K-edge) in the X-ray absorbing atom, $F_j(k)$ is the backscattering amplitude (called the amplitude function) for each atom in the $j$th shell, $R_j$ is the root mean square distance between the central atom and each atom in the $j$th shell, $\sigma_j$ is the Debye–Waller factor which measures the variation in $R_j$ about its mean, $\lambda_j$ is the electron mean free path, and $\phi_{ij}$ is the phase shift (called the phase function) experienced by the photoelectron, which is a function of both the absorbing $i$ atom and backscattering atom. In eq 1 it has been assumed that $R_j$ and the type of atom are identical for all atoms in the $j$th shell. (Actually, $R_j$ does not necessarily need to be identical, since slight variations in $R_j$ between different atoms in the same shell can be accounted for by the Debye–Waller factor.) If the material or the electric field polarization is isotropic, then the sum over $l$ can be performed and the result is $N_j$, the number of atoms in the $j$th coordination shell. $k$ is called the wavevector because $2\pi/k$ is the wavelength of the ejected photoelectron. Through a simple energy balance it can be shown that

$$k = \left[\frac{2m_e}{\hbar^2}(E - E_0)\right]^{1/2} \quad (2)$$

where $E_0$ is the absorption edge energy, $m_e$ is the mass of an electron, an $\hbar$ is Planck's constant divided by $2\pi$.

Equation 1 gives the expression for EXAFS oscillations as a function of wavevector, but generally a Fourier transformation is performed to yield the radial structure function (RSF). The RSF is similar to a radial distribution function in that peaks in the RSF correspond to distinct coordination shells. The units of the abscissa of the Fourier transform are angstroms, but the peaks are shifted from the interatomic distances as indicated by eq 1; hence a subscript F will be used to distinguish this distance from the actual interatomic distance $R$.

BAN, available from Tolmar Instruments, was used for converting the measured $\mu t$ vs $E$ curve to $k^2\chi(k)$ vs $k$, subsequent Fourier transformation, isolation of each shell, back transformation, and determination of the four unknown EXAFS parameters. This software uses the ratio method[6] to calculate $N/N_{ref}$, $E_0 - E_{0,ref}$, $\sigma^2 - \sigma_{ref}^2$, and $R - R_{ref}$ for each shell, where the subscript ref represents the value for the unstretched material. Details of coordination structure determination are given in the first paper in this series.

Equation 1 can be written in the form

$$\chi(k) \propto (\mu_c \cdot \mathbf{E}) \quad (3)$$

where $\mu_c$ is the vector from the central atom to the $l$th atom in the $j$th coordination shell an $\mathbf{E}$ is the polarization direction of the X-rays. This equation is analogous to the expression for the absorption of infrared radiation:

$$A \propto (\mu \cdot \mathbf{E}) \quad (4)$$

where $A$ is the measured absorbance, $\mu$ is the dipole moment of the molecular vibration, and $\mathbf{E}$ is the polarization direction of the infrared radiation. Therefore, to analyze the directionally dependent EXAFS data, the formulas which have been derived for infrared dichroism can be adapted for these experiments.

In infrared dichroism experiments, the absorbance of radiation is measured with the electric field vector parallel and perpendicular to the stretch direction, and the second moment of the orientation function $\langle P_2(\cos\theta)\rangle$ for the chain axis can be written[7]

$$\langle P_2(\cos\theta)\rangle = \frac{(R-1)(R_0+2)}{(R+2)(R_0-1)} \quad (5)$$

where $R_0$ is given by $2\cot^2\alpha$ ($\alpha$ is the angle between the chain axis and the dipole moment vector) and $R$ is defined as

$$R = A_{\parallel}/A_{\perp} \tag{6}$$

where $A_{\parallel}$ is the absorbance when the stretch direction and the polarization direction are parallel and $A_{\perp}$ is the absorbance when the two directions are perpendicular.

To use eq 5 to analyze EXAFS experiments, it is simplest to consider the case where none of the other parameters appearing in eq 1 besides $\theta_{ij}$ are different within shell $j$ for each sample. The left side of eq 3 is a function of a variable $k$; however, if all the other parameters in eq 1 are unaffected, then changes in the orientation simply scale the oscillations. This scaling is like multiplying a sine wave by a constant, which simply changes the amplitude without changing the period or the phase shift. In the cases where other parameters are affected, this formalism still applies because the analysis explicitly accounts for other changes. However, the term containing the electron mean free path was not adjusted for changes in $R_j$, so if the parallel and perpendicular samples had different $R_j$ values, then this analysis is incorrect. As will become evident, any differences in $R_j$ were extremely small and thus an insignificant source of error.

In EXAFS experiments, the dipole moment vector does not exist and eq 5 can be written

$$\langle P_2(\cos\theta)\rangle = \frac{R-1}{R+2} \tag{7}$$

where $R$ is given by

$$R = \frac{(N/N_{ref})_{\parallel}}{(N/N_{ref})_{\perp}} \tag{8}$$

In this case $\langle P_2(\cos\theta)\rangle$ represents the second moment of the orientation function for the coordination bond vectors.

All error bars shown in this paper represent two standard deviations. When the data clearly indicated no change in $R$ as the draw ratio increased, all samples were averaged to calculate the mean and standard deviation of $R$. Error bars for $N/N_{ref}$ and $\sigma^2-\sigma_{ref}^2$ were calculated in two different ways for the nickel- and zinc-neutralized samples. Since both parallel and perpendicular spectra were collected for the unstretched sample, the standard deviation could be calculated from these two samples. This value was approximately two-thirds of the value from the second method. In the second method, three NiSPS samples were stretched to $\lambda = 2.5$ and the results were used to calculate the standard deviation. These values represent an upper limit since the samples had slipped slightly in the grips (these samples were the first ones stretched and shortly thereafter the grips were modified to eliminate slippage) so that the final elongations varied by approximately 10%. Since the signal to noise ratio was much smaller for the cadmium-neutralized samples, the error for these samples was calculated from the unstretched samples as well as from two samples which had both been stretched to a draw ratio of 4.5. The standard deviations were approximately equal for the two methods in the cadmium-neutralized material.

## Results

**ZnSPS.** As described in the previous paper, zinc is surrounded by four oxygen atoms from sulfonate groups. The distance between zinc and oxygen in the unstretched material is 1.954 Å based on the average of the parallel and perpendicular EXAFS spectra of the unstretched material. As Figure 1 shows, this distance increases up to $\lambda \approx 1.5$ and then plateaus when the sample is analyzed with radiation polarized parallel to the draw direction. The distance also seems to increase perpendicular to the draw direction as well, although the shift is not as great and some doubts remain whether this difference is outside experimental error. Since two standard deviations for the NiSPS samples and the CdSPS samples as well as for the unstretched zinc material was about 0.01 Å, there is great confidence in the error bars shown in Figure 1 and the increase in bond distance parallel to the draw direction is beyond statistical variation. $R_F$ corresponding to the peak position clearly increases upon stretching as shown in Figure 2, which confirms the results of the analysis presented in Figure 1. The peak shape and height clearly are altered as well, which indicates a change in either the Debye–Waller factor and/or the alignment of bond vectors. Figure 3 shows how $N/N_{ref}$ and $\sigma^2-\sigma_{ref}^2$ are modified by

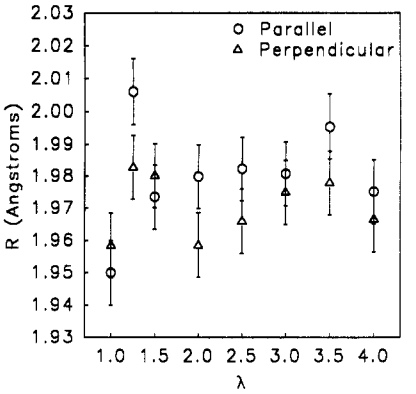


**Figure 1.** Variation of the ZnO first coordination shell distance after uniaxial orientation in ZnSPS.

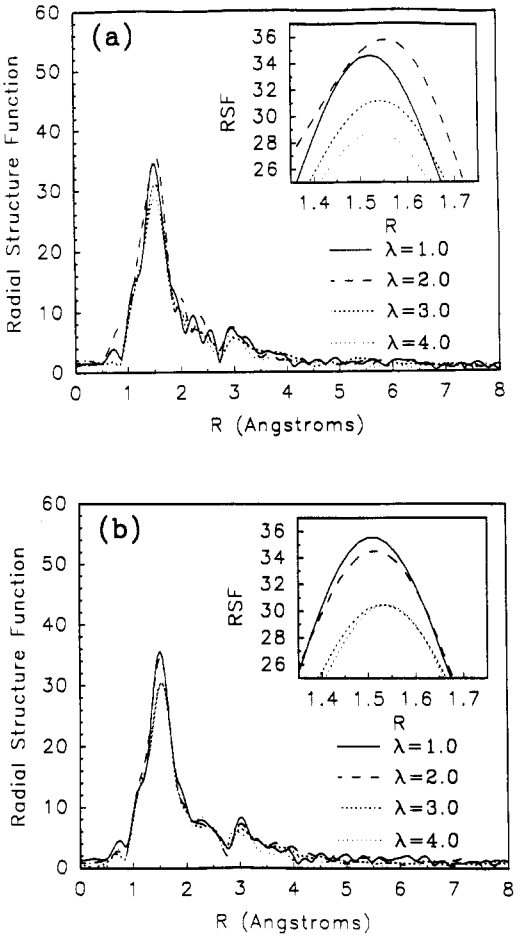


**Figure 2.** RSF for selected draw ratios for ZnSPS: (a) RSF when the draw direction and the X-ray electric field vector are parallel; (b) RSF when the two are perpendicular.

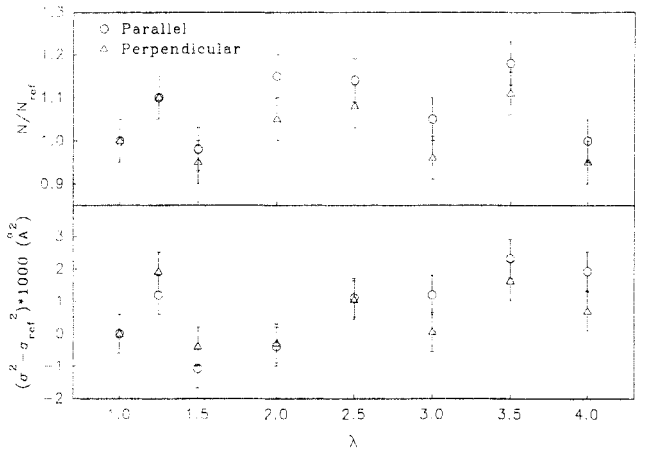


**Figure 3.** $N/N_{ref}$ and $\sigma^2 - \sigma_{ref}^2$ for ZnSPS as a function of draw ratio.

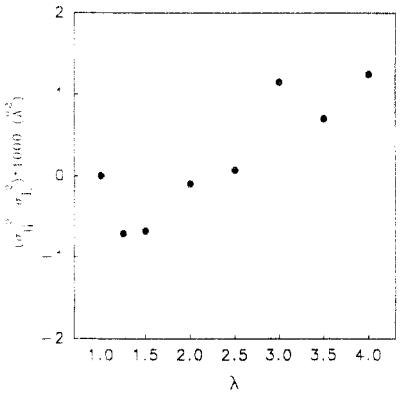


**Figure 4.** $\sigma_\parallel^2 - \sigma_\perp^2$ for ZnSPS as a function of draw ratio.

uniaxial extension. In neither case could it be concluded that the difference relative to the undrawn material was outside of experimental error, although both are close to being statistically significant.

The relevant information contained in Figure 3 is not only in the absolute difference relative to the undrawn material but also in the parallel and perpendicular values at a single draw ratio relative to each other. As can be seen by inspection, the ratio of the parallel data to the perpendicular data follows a well-defined pattern for the change in the number of atoms; the parallel $N/N_{ref}$ was always greater than the perpendicular $N/N_{ref}$ for $\lambda > 1.25$. This consistency coupled with the conservative estimation of the error suggests very strongly that this effect was real. A comparison of parallel and perpendicular values for the change in the Debye–Waller factor gives the result shown in Figure 4. Although the trend is well-defined, the complexity of the pattern coupled with the noise and the number of data points makes it difficult to draw conclusions from these data. However, if one were to believe the trend, Figure 4 indicates that the disorder first decreases at low elongations and then increases as the elongation increases further.

Assuming that the Zn–O bond distance was not different for the parallel and perpendicular sets of EXAFS data, one can apply the formalism introduced in the preceding section to determine the second moment of the orientation function for the Zn–O coordination bonds. The second moment of the orientation function is shown in Figure 5 and exhibits a very rapid increase at low elongations and then plateaus as the sample is stretched further. This qualitative behavior agrees very well with the behavior for polyurethane ionomers discussed in the Introduction.

**NiSPS.** The perpendicular NiSPS EXAFS data showed extremely unusual behavior as illustrated in Figure 6.

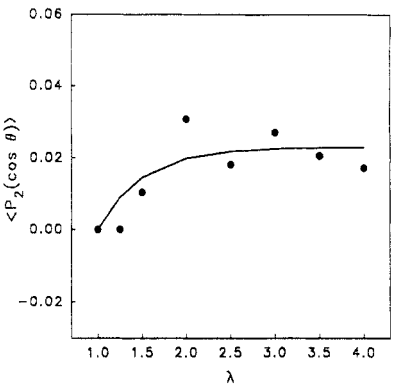


**Figure 5.** Second moment of the orientation function for ZnO coordination bond vectors as a function of draw ratio in ZnSPS. The solid line represents a possible smooth curve which describes the change in the orientation with draw ratio.

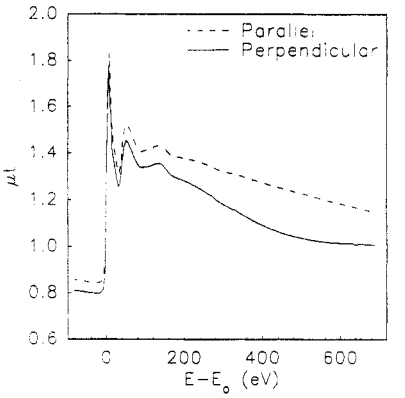


**Figure 6.** Raw $\mu t$ vs energy data for NiSPS with the X-ray electric field vector and the draw direction perpendicular ($\lambda$ = 2.5).

Essentially, the absorption coefficient for the perpendicular samples was highly curved in the EXAFS region. As a quick inspection of eq 1 illustrates, isolation of the EXAFS oscillations requires a precise definition of the average absorption coefficient. Thus it was not possible to determine the mean absorption coefficient for the perpendicular data sets. This curvature was only found for this particular set of nickel-neutralized samples. Also, the unstretched samples did not show this curvature, and the curvature became more pronounced as the draw ratio increased.

Therefore, only results with the electric field and the polarization direction parallel are presented. In NiSPS, three RSF peaks were visible with the first due to octahedral coordination to oxygen (distance = 2.04 ± 0.01 Å) and the second due to sulfur (distance = 3.24 ± 0.01 Å). The third shell is too weak to analyze by the ratio method. Figure 7 shows RSFs for NiSPS as a function of draw ratio. Figure 8 clearly indicates that the distances for the first and second shells were unchanged after stretching. Figure 9 indicates that a change probably occurred in the Ni–O bond vector alignment. Although the differences were not much greater than experimental error, the absence of changes in the second shell shown in Figure 10 supports the conclusion that the changes in the first shell were real. $\sigma^2 - \sigma_{ref}^2$ presented in Figure 9 indicate that an increase in the amount of disorder may also have occurred in the first shell.

Although the analysis suggests that the Ni–S second shell was not affected by macroscopic uniaxial orientation, one cannot be absolutely certain about this conclusion. As discussed in the previous paper, the second-shell sulfur peak has a significant contribution from nearby oxygen

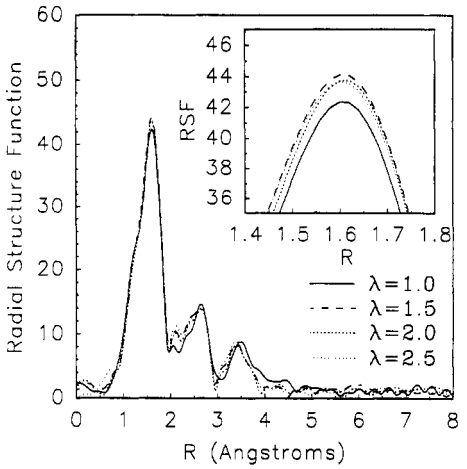


**Figure 7.** RSF for NiSPS with the X-ray electric field vector and the draw direction parallel at various draw ratios.

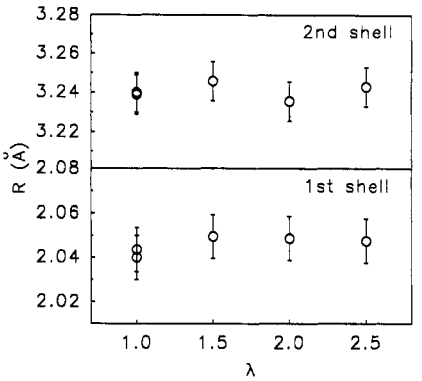


**Figure 8.** Variation of the NiO first coordination shell distance and the NiS second coordination shell distance in NiSPS after uniaxial orientation with the X-ray electric field vector and the draw direction parallel.

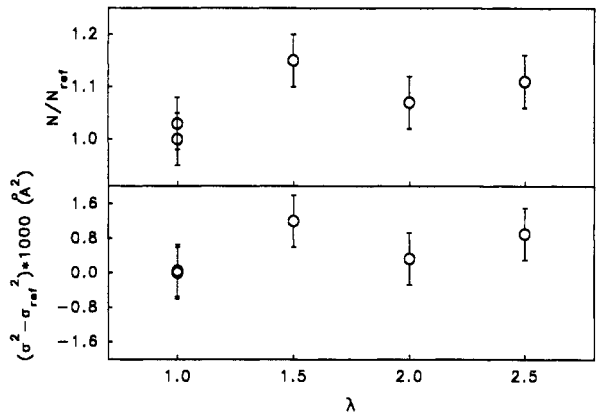


**Figure 9.** $N/N_{ref}$ and $\sigma^2 - \sigma_{ref}^2$ for NiO in NiSPS as a function of draw ratio with the X-ray electric field vector and the draw direction parallel.

atoms. The backscattering from these oxygen atoms destructively interferes with sulfur backscattering, which serves to reduce the height of the second-shell sulfur peak. It is possible that a shift in Ni–O third-shell alignment compensates for a shift in Ni–O second-shell alignment. However, given the rather stringent requirements under which oxygen partially cancels sulfur backscattering, one would expect that the second shell was not affected by bulk uniaxial extension.

**CdSPS.** RSFs for selected samples shown in Figure 11 exhibit only one clear coordination shell, which is due to octahedrally coordinated oxygen (distance = 2.34 Å). Simulations discussed in the previous paper indicate that two oxygens are from water and four are from sulfonate

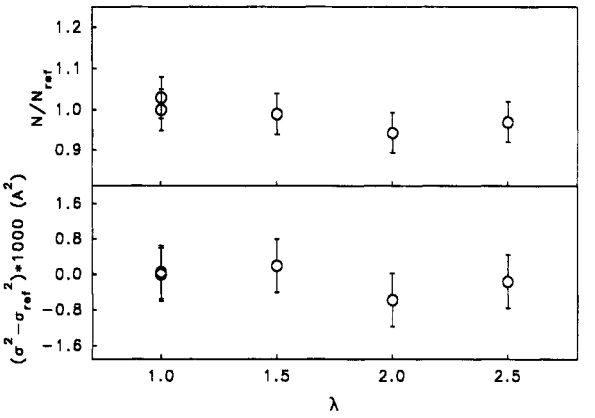


**Figure 10.** $N/N_{ref}$ and $\sigma^2 - \sigma_{ref}^2$ for NiS in NiSPS as a function of draw ratio with the X-ray electric field vector and the draw direction parallel.

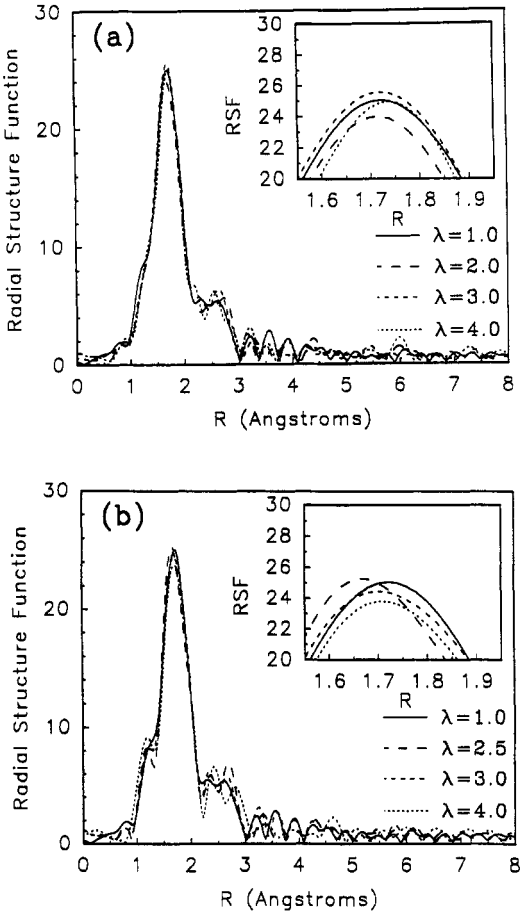


**Figure 11.** RSF for selected draw ratios for CdSPS: (a) RSF when the draw direction and the X-ray electric field vector are parallel; (b) RSF when the two are perpendicular.

groups. The best fit results for nickel- and zinc-neutralized materials contain no oxygen from water. As one might ascertain from Figure 11, no changes occurred in any of the EXAFS parameters as indicated by Figures 12 and 13. Comparison of Figures 11–13 with their counterparts for zinc clearly show that no consistent trends or changes are found for the cadmium ionomer in contrast to the zinc ionomer.

## Discussion

Figures 5 and 9 suggest that the change of the local coordination environment occurs rapidly upon stretching and reaches a plateau between λ = 1.5 and λ = 2. Both SAXS and SANS experiments on uniaxially deformed sulfonated polyurethanes presented in the Introduction

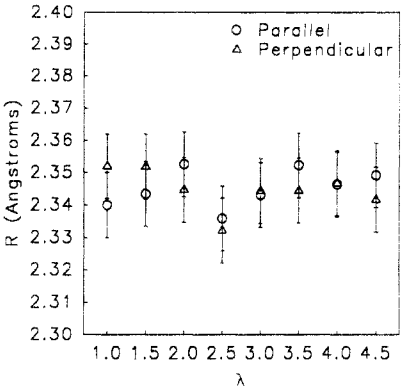


**Figure 12.** Variation of the CdO first coordination shell distance after uniaxial orientation in CdSPS.

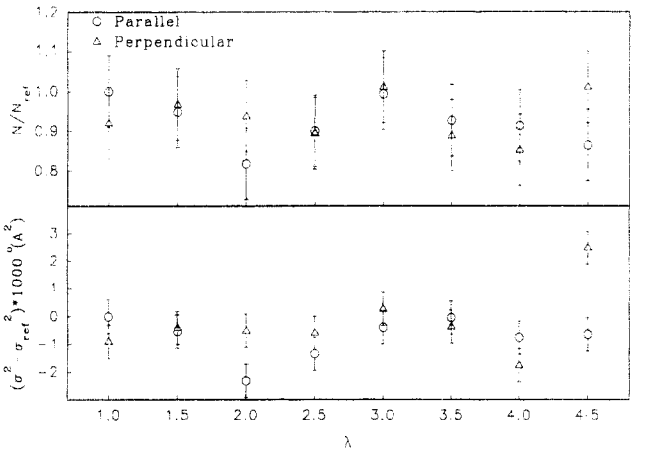


**Figure 13.** $N/N_{ref}$ and $\sigma^2 - \sigma_{ref}^2$ for CdSPS as a function of draw ratio.

also show a transition near $\lambda = 1.5$–2 in the response of ionomers to an applied external stress. The qualitative agreement between the SAXS, SANS, and EXAFS results suggests that responses of the polyurethane and the polystyrene ionomers to stress are similar, if not identical. A qualitative model has been previously presented based on the results of the SAXS and SANS deformation experiments.[8] These authors postulated that at low elongations, aggregates rearrange in the polymer matrix without chain stretching while at higher elongations, chains will stretch because aggregate rearrangement is no longer possible. In order for aggregate rearrangement to occur without chain stretching at low elongations, the aggregates cannot be true cross-links; i.e., ions must be able to disassociate from the aggregate and move to either a different aggregate or form a new aggregate with other ions. This suggests that the aggregates are much more fluid than previously suspected.

In this study, the response of the intra-aggregate environment to uniaxial orientation was followed. We believe the underlying cause of bond vector alignment was aggregate deformation. The only mechanism by which bonds can become aligned is through changing of oxygen–metal–oxygen angles, which will be termed bond bending. Further, it seems extremely likely that the cause of this bending is aggregate deformation. As an example, consider initially spherical aggregates being deformed into ellipsoids. Clearly, the bonds inside the aggregate must bend to accommodate this shape change.

One might think that the alignment of bond vectors could be from the alignment of anisotropic aggregates. However, for tetrahedral as well as octahedral coordination, it is not possible to cause a preferential alignment of metal–oxygen bond vectors along a single axis by rotation alone. Unless the immediate coordination environment is anisotropic, which is extremely unlikely, simply aligning aggregates could not explain the experimental results. This reasoning is not meant to imply the aggregates themselves are isotropic; in fact, the unit cell which would correspond to Figure 4 of the previous paper is highly anisotropic; however, the metal–oxygen bonds are not.

Unfortunately, bond bending is inconsistent with the SANS results since chain stretching must be stressing the aggregates to cause deformation. Comparing polystyrene ionomers with polyurethane ionomers is not as unreasonable as one might expect: both were stretched at ~80 °C above the glass transition, in the cases of PTMO-1000 both continuous phases were amorphous, the weight fraction of ionic groups were not greatly different, and the polydispersity of PTMO was about 1.5[8] so the distance between ionic groups was not uniform in either case. Rather, the greatest difference between the two studies was procedural since the polyurethane ionomers were allowed to relax for 30 min prior to measurement, while the materials in the present study were quickly quenched below their glass transition temperature after stretching. The results of both studies can be reconciled if one assumes that the initial stretching deforms the aggregates and stretches the chains, while at longer times redistribution of the ions can relieve the stress and eliminate any chain stretching. This distribution causes the change in Bragg spacing discussed in reference to SAXS studies. At higher elongations, this relaxation process cannot totally relieve chain stretching and the chain segments retain some level of orientation.

The cation type was found to be an important factor in the response of the local environment to stress. The zinc material clearly exhibited orientation of the bond vectors as well as a lengthening of the first coordination bond. The nickel ionomer showed the former without the latter. Finally, the cadmium material was not affected by the macroscopic elongation. Perhaps the lack of orientation in the cadmium ionomers was related to the presence of water in the immediate coordination environment since clear evidence of water was not found for the other two cations.[4] Water plasticizes the aggregates and allows the ionomer to relax more easily, which perhaps relieves the stress on the aggregates and explains why the cadmium coordination environment was not anisotropic.

It was hoped that these studies might offer direct insight into the relaxation mechanisms in ionomers. Rather than the nomral slow diffusional process through the matrix, ionomers are thought to relax via hopping of ions from one aggregate to another. No change was found in the average environment around a cation, which suggests that the local environment is unchanged after hopping occurs. Given the highly ordered local structures, it is hard to believe that ions migrating from one aggregate to another do so without some loss in local order. There are a number of possible explanations why such a loss of order was not observed in the present study. It is possible that the time scale of rearrangement inside the aggregates is much faster than a few seconds or the local environment can rearrange even when the polymer is glassy since motion is required only over a few angstroms. Another possibility is that the less-ordered counterions which exist on the periphery of the aggregate are hopping while the well-ordered interior ions are not. A final possibility is that the hopping may not be occurring in this experiment since the model presented earlier suggests that this hopping occurs over longer time scales than a few seconds.

## Conclusions

The response of the cation coordination structure to uniaxial deformation has been measured in three sulfonated polystyrenes. None of the materials showed dramatic changes after stretching. For the zinc-neutralized material, the first-shell Zn–O distance parallel to the draw direction increased by approximately 0.02 Å and the Zn–O bond vectors aligned in the stretch direction. The alignment was quantified through the use of the second moment of the orientation function of the bond vectors. For nickel-neutralized materials, the data collected when the electric field vector and the orientation axis were perpendicular were unusable. Data collected when the two were parallel indicated that the same first-shell Ni–O alignment occurred in this system; however, the absolute difference was on the order of the experimental error. No alignment was observed in the second-shell Ni–S distance,and no change was found in either the first- or second-shell distances. In the cadmium-neutralized material, where the unoriented structure had clear evidence of waters of hydration, there was no response of the local structure to orientation.

**Acknowledgment.** This study would not have been possible without the extremely helpful personnel at CHESS. We thank Rich Goddard for assisting with EXAFS experiments and Mr. Matt Newville at the University of Washington for his help concerning FEFF5. Financial support for this work came from the Department of Energy under Grant DE-FG02-88ER45370. B.P.G. thanks the Department of Defense for its fellowship support through the National Defense Science and Engineering Graduate Fellowship program.

## References and Notes

(1) Ding, Y. S.; Hubbard, S. R.; Hodgson, K. O.; Register, R. A.; Cooper, S. L. *Macromolecules* **1988**, *21*, 1698.
(2) Visser, S. A.; Cooper, S. L. *Polymer* **1992**, *33*, 4705.
(3) Visser, S. A.; Pruckmayr, G.; Cooper, S. L. *Polymer* **1992**, *33*, 4280.
(4) Grady, B. P.; Cooper, S. L. *Macromolecules*, previous paper in this issue.
(5) Ken Fenkelstein, private communication.
(6) Teo, B. K. *Infrared Spectroscopy of Polymers*; Springer-Verlag: New York, 1986.
(7) Zbinden, R. *Infrared Spectroscopy of Polymers*; Academic Press: New York, 1964.
(8) Visser, S. A.; Cooper, S. L. *Polymer* **1992**, *33*, 920.